



Experimental study of water-based CuO nanofluid flow in heat pipe solar collector

Mohammad Shafiey Dehaj³ · Mostafa Zamani Mohiabadi^{1,2}

Received: 14 August 2018 / Accepted: 26 January 2019 / Published online: 2 March 2019
© Akadémiai Kiadó, Budapest, Hungary 2019

Abstract

The main goal of this study is the experimental evaluation of the thermal performance of heat pipe solar collector (HPSC) at different high flow rates of water and CuO–water nanofluid with various volume fractions. In this regard, a test bench of the HPSC was manufactured and tested in the laboratory of Vali-e-Asr University, while the co-precipitation method was used to prepare CuO nanoparticles. The structural and optical properties of the nanostructure were characterized by means of X-ray diffraction, Fourier transform infrared spectroscopy, scanning electron microscopy, and UV–visible analysis. The collector efficiency and pumping power were calculated for nanofluids, and the results were compared with ones of water working fluid; based on the experimental results, copper oxide nanofluid and deionized water at a volume fraction of 0.017 and a flow rate of 14 L min⁻¹ yields the greatest improvement in the efficiency of the solar collector. The results also showed that the efficiency of solar collector increases with the flow rate and the volume fraction of the nanofluid.

Keywords Metal oxides · Nanoparticles · Nanofluids · Renewable energy · Experimental collector efficiency

List of symbols

A_c	Surface area of collector (m ²)
C_p	Specific heat capacity (J kg ⁻¹ K ⁻¹)
D	Crystal size (nm)
d	Diameter of the pipe (m)
f	Friction factor
G	Solar radiation (W m ⁻²)
k	Shape factor
K	Thermal conductivity (W m ⁻¹ K ⁻¹)
L	Length of the pipe (m)
\dot{m}	Mass flow rate (kg s ⁻¹)
Δp	Pressure drop (Pa)
Q_u	Heat gain of the working fluid (W)

Re	Reynolds number
T	Temperature (K)
T_a	Environment temperature (K)
V	Velocity (m s ⁻¹)
\dot{W}	Pumping power (W)

Greek symbols

α	The ratio of thermal conductivities (K_{np}/K_{bf})
β	Full width at half maximum (FWHM)
ϕ	Volume fraction (%)
η	Thermal efficiency
η_0	Maximum thermal efficiency
λ	Wavelength of the X-ray source (nm)
μ	Viscosity (kg ms ⁻¹)
θ	Bragg diffraction angle
ρ	Density (kg m ⁻³)

✉ Mostafa Zamani Mohiabadi
m.zamani@vru.ac.ir

Mohammad Shafiey Dehaj
m.shafiey@vru.ac.ir

¹ Department of Chemical Engineering, Faculty of Engineering, Vali-e-Asr University of Rafsanjan, Rafsanjan, Iran

² Department of High Temperature Fuel Cell, Vali-e-Asr University of Rafsanjan, Rafsanjan, Iran

³ Department of Mechanical Engineering, Faculty of Engineering, Vali-e-Asr University of Rafsanjan, Rafsanjan, Iran

Subscripts

bf	Base fluid
nf	Nanofluid
np	Nanoparticles
i	Inlet
o	Outlet

Introduction

Nowadays, one of the main concerns is the increase in energy demands while fossil fuels are depleting. The renewable energies, such as solar energy, can serve as one of the best choices to deal with this concern, whereas solar collectors are receiving serious attention for supplying indoor hot water to buildings [1]. Given the importance of this kind of solar systems, extensive research has focused on improving the efficiency of solar collectors.

The heat pipe and the flat plate are mostly used in solar systems for heating and cooling of buildings [2]. Among different stationary solar collectors, HPSCs are commonly applied because of their easy installation, good efficiency, reliability, transportation (handling), and economic and environmental advantages [3–6].

One of the most recent methods to enhance the performance of the collectors is the use of nanofluids as the working medium. Nanofluids refer to a relatively new class of fluids that consist of a base fluid containing suspended particles (metals or metal oxides) in nanosizes (1–100 nm). He et al. [7] evaluated the thermal performance of solar flat plate collector with Cu–H₂O nanofluid as its working fluid experimentally. The results showed that the small size of the nanoparticles increased the efficiency of the collector. They compared the results with the base fluid.

New descendants of heat transfer fluids, such as nanofluids, are proven to be promising for future applications in solar collectors [8]. Adding nanoparticles into a base fluid has several dominant characteristics that are the result of the small size and thermophysical properties of the nanoparticles [9].

The first stage in the preparation of nanofluids is their synthesis. Chemical, physical, and biological methods can be implemented to synthesize nanoparticles. Fuskele et al. [10] have explained some methods of nanoparticle synthesis.

Generally, two methods are applied to produce nanofluids: (a) a single-step method and (b) a two-step method. The single-step method combines the preparation of nanoparticles with the synthesis of nanofluids in which the nanoparticles are directly prepared by using physical vapor deposition procedure. But in the two-step method, the nanoparticle preparation step is separated from the nanoparticle dispersion step [11].

Sundar et al. [12] reviewed the correlations developed for the evaluation of the Nusselt number and friction factor of the nanofluid flowing in the solar collectors with various types of inserts. They asserted that the disadvantage of the two-step method was that only low-vapor-pressure fluids were compatible with the technique.

The experimental studies showed that the dispersal of small amounts of nanoparticles in the base fluids significantly enhances the thermal conductivity and thermal performance of the heat transfer systems [13]. Nagarjan et al. [14] reviewed solar systems with a focus on the application of nanofluids and their thermophysical properties.

Likewise, Ahmad [15] extensively reviewed recent developments in the application of nanotechnology in solar collectors. He covered theoretical, numerical, and experimental studies that addressed the employment of nanotechnology in flat plates and heat pipe solar collectors. The findings of scholars were thoroughly tabulated to present an overview of the exploitation of nanofluids in solar collectors and their major impacts on the enhancement of the efficiency of solar collectors.

In addition, Mahmud et al. [16] reviewed the latest developments in the application of nanofluids in stationary solar systems. They studied the effects of nanofluid employment in solar collectors from economic and environmental perspectives.

An HPSC was designed and fabricated by Daghigh et al. [17]. They firstly extended a mathematical model and then, they tested the system experimentally. The thermal performance of the HPSC was evaluated against various parameters such as the mass flow rate of working fluid and number of heat pipes.

Milanese et al. [18–20] investigated the layering phenomenon at the liquid–solid interface and optical absorption on various water-based nanofluids and metal oxide nanoparticles. The results showed that layers of ordered water molecules surrounding metal nanoparticles had significant effects on explaining experimental data of nanofluid thermal conductivity. They reported that the material and concentration of nanoparticles considerably influenced the optical behaviors of the nanofluids. Also, they presented the results as a function of temperature to obtain a better understanding of optical properties.

Colangelo et al. [21] used a commercial software package (RadTherm Thermo Analytics rel. 10.5) to estimate the potential efficiency of an innovative HPSC. They used CuO and Al₂O₃ nanofluid as the nanoadditives and compared numerical results with experimental findings.

Mirzaei [22] conducted an experimental investigation into the thermal performance of a flat plate solar collector by using CuO–water nanofluid with various mass flow rates while the volume fraction of the CuO nanoparticles was kept constant. He showed that for all of mass flow rates, the collector's efficiency improved to a greater extent using nanofluid than that of pure water.

The application and effect of nanofluids as working fluids in solar systems were reviewed by Mahian et al. [23] and Verma et al. [24]. Mahian et al. studied the efficiency

of solar collectors in terms of economic nanofluids and environmental consideration.

Moghadam et al. [25] studied the effects of CuO–water nanofluid as a working fluid on the thermal performance of a solar flat plate collector. In their study, the volume fraction was set at 0.4%, the particle dimension was 40 nm, and the flow rate was set at 1–3 kg min⁻¹. The results revealed that the efficiency of the collector increases with the flow rate.

Sadri et al. [26, 27] developed a facile, bio-based, environmentally friendly method to synthesize well-dispersed clove-functionalized multi-walled carbon nanotubes (C-MWCNTs) and clove-treated graphene nanoplatelet (CGNP) coolants. Their results showed that this technique increases the thermophysical properties and stability of the MWCNTs in aqueous media. Also, they prepared the CGNP/water nanofluids at three different volume fractions and tested this nanofluid in a horizontal tube heat exchanger. They evaluated heat transfer and hydrodynamic characteristics of the CGNP/water nanofluids. Hosseini et al. [28] performed a numerical simulation of convection heat transfer and hydrodynamic properties of a concentric annular heat exchanger for which they used nanofluids containing the C-MWCNTs with different volume fractions as the working fluids. Also, by using ANSYS Fluent computational fluid dynamics software, they developed a three-dimensional model of this type of heat exchanger for turbulent flow. They compared and validated the results of simulation with experimental data at different Reynolds numbers and particle concentrations of the C-MWCNTs.

Above review of the available literature shows that a few studies have focused on the HPSCs. Correspondingly, most of the past studies have considered the efficiency of solar collectors in different low flow rates of the base fluids and nanofluids as the working fluid. The main purpose of the present study is to experimentally evaluate the efficiency of a heat pipe solar collector at different high flow rates of pure water and CuO/water nanofluid with various volume fractions as working fluids as well as the preparation and synthesis of the CuO nanofluids. As a test bench, the HPSC was manufactured and tested in the laboratory of Vali-e-Asr University to explore the thermal performance of the HPSC at different nanoparticle volume fractions.

Experimental

Heat pipe solar collector description

A setup of HPSC was designed, built, and tested in the solar laboratory of Vali-e-Asr University of Rafsanjan (Lat. 30.35°N; Long. 56.00°E). The collector was oriented at the

tilt angle of 45° in Rafsanjan city, which has semiarid weather conditions. The experimental setup, including a closed loop of solar collector coupled with a storage tank and instruments, was built as shown in Fig. 1a, while Fig. 1b depicts the schematic diagram of the given solar collector.

During the tests, the inlet and outlet flow temperatures of the solar system, mass flow rate, environment temperature, and solar radiation density were measured. The specifications of the heat pipe are presented in Table 1.

The working fluid was fed to the panel using a centrifugal pump (power 120 W, capacity 40 L min⁻¹, head 9 m). The flow rate of the water through the collector was regulated by a simple manual valve with a maximum 20 L min⁻¹ mass flow rate. The reservoir tank was coupled with a closed loop of the working fluid of the collector circle. The tank capacity was about 12 L. The flow rate was measured with a rotameter placed vertically at the outlet of the collectors. The collectors were instrumented with *T*-type thermocouples (– 250 to 400 °C) to measure temperatures of the working fluid at the inlet and outlet of the collector. A thermocouple was used to measure the environment temperature; however, to minimize the effect of the direct sunlight, it was covered with a shelter. The intensity of total solar radiation was recorded using a digital solar meter (1–1300 W m⁻²). All the sensors used in the collector continuously monitored the system, while the output signals were recorded in a data acquisition system every 5 min. More details are given in [22].

Thermal performance of HPSC

Experiments were done at the same time periods between 08:00 and 12:00 and between 14:00 and 17:00 under Rafsanjan weather conditions, and the test results were sampled for two random days of each month (total 24 days). The flow rate of the working fluids was 5, 8, 11, and 14 L min⁻¹. The collecting efficiency, working fluid temperature, and heat gain were compared in the same solar irradiation. The heat gain of the working fluids can be obtained by the following equation:

$$Q_u = \dot{m}C_p(T_o - T_i) \quad (1)$$

The efficiency of the collector is defined by ASHRAE Standard 93-86 as the energy absorbed by the fluid (collector) divided by the incoming thermal flow (solar intensity) to the collector [29]. The thermal performance of collector η_i can be calculated by Eq. (2)

$$\eta_i = \frac{\text{useful gain}}{\text{available energy}} = \frac{Q_u}{A_c G} = \frac{\dot{m}C_p(T_o - T_i)}{A_c G} \quad (2)$$

Metallic nanofluids improve thermophysical properties such as thermal conductivity, density, viscosity, and

Fig. 1 Setup of the system at solar site of Vali-e-Asr university of Rafsanjan; **a** experimental setup, **b** simplified closed-loop system



Table 1 Solar collector parameters

Item	Value
Number of tubes	15
Gross area	3.27 m ²
Absorber area	1.56 m ²
Mass	60 kg
Dimensions	1990 × 1640 mm
Max working pressure	6 bar
Max stagnation temperature	250 °C
Absorber coating	SS-ALN-CU ($\sigma > 0.95$ $\varepsilon < 0.05$)
Long-term vacuum	10 ⁻⁸ bar
Frost resisting	- 50 °C
Max. working temp.	300 °C
Hail resistance	Ø35 mm
Manifold shell	Frosted aluminum alloy (grey or black painting)
Insulation	Rock wool, 50 mm thickness, 180 kg/m ³
Frame	Aluminum alloy
Recommended installation angle	15°–90°

specific heat capacity as compared to pure fluids such as oil or water. The thermophysical properties of the nanofluids are related to the properties of the base fluid and nanoparticles. The effective thermal conductivity of the nanofluids is calculated by Eq. (3) (Maxwell’s model) [30]:

$$\frac{K_{nf}}{K_{bf}} = 1 + \frac{3(\alpha - 1)\phi}{(\alpha + 2) - (\alpha - 1)\phi} \tag{3}$$

The general formulas for the density and viscosity (Batchelor’s model) as the thermophysical properties of the nanofluids can be estimated through the below formula:

$$\mu_{nf} = (1 + 2.5\phi + 6.2\phi^2)\mu_{bf} \tag{4}$$

$$\rho_{nf} = \rho_{np}\phi + \rho_{bf}(1 - \phi) \tag{5}$$

In solar system, an electrical powered pump is needed to pump the working fluid in the HPSC. The pressure drop is evaluated by the following formulas:

$$\Delta p = f \frac{L\rho V^2}{d}, \quad f = 0.3164 Re^{-0.25}; \tag{6}$$

therefore, the pumping power can be calculated by the following equation [31]:

$$\dot{W} = \left(\frac{\dot{m}}{\rho}\right)\Delta p \tag{7}$$

Finally, for constant Reynolds number, the relative pumping power can be obtained using [32]:

$$\frac{\dot{W}_{nf}}{\dot{W}_{bf}} = \left(\frac{\rho_{bf}}{\rho_{nf}}\right)^2 \left(\frac{\mu_{nf}}{\mu_{bf}}\right)^3. \tag{8}$$

Preparation of nanofluid CuO and deionized water

Cupric nitrate trihydrate [Cu(NO₃)₂·3H₂O], polyethylene glycol (PEG-400) [H(OCH₂CH₂)_{Noh}], and sodium hydroxide pellets (NaOH) were in high quality and analytical reagent grade quality. Deionized water was used throughout the experiments.

The main step in the experimental investigations on nanofluids is nanofluid preparation. There are two different approaches to the production of nanofluids: the single-step method and the two-step method. The two-step method is the most common and cost-effective approach to the preparation of nanofluids. The sediment of nanoparticles to the aggregation is high because of their surface activity as well as their large surface area [33].

To prepare CuO nanofluids, an amount of 0.1 g [Cu(NO₃)₂·3H₂O] was dissolved in 40 mL of deionized (DI) water and was mixed with a stirrer. An amount of 0.1 g of polyethylene glycol (PEG-400) was added as a surfactant. A little aqueous solution of NaOH was added

slowly (drop-wise) into the solution. When pH 10, the solution gets opalescent color, and then, the container is removed from the stirrer. An amount of ethanol was added to the solution, and it was kept at room temperature for 1 day so that its water was evaporated as much as possible. Also, the water in the solution was removed. Then, the solution was mixed through oven-dried at 120 °C for 3 h in order to evaporate its water. After that, it was cooked in an oven at 600 °C for 3 h. When the temperature of the furnace reached the ambient temperature (about 3 h), the container removed from the furnace. Copper oxide nanoparticles were ready [34].

An amount of 2 L of deionized water was placed in a container and was added to 1 g of CuO nanoparticles. Then, it was placed on the stirrer. Adding the suitable surfactants to the base fluids can stabilize the nanofluids by reducing surface tension and increasing the immersion of the nanoparticles which contributes to avoid sedimentation. Researchers have used various kinds of suitable surfactants for the stabilization of nanofluids [10]. Thus, to prevent agglomeration and sedimentation of the nanoparticles, 0.2 g of polyethylene glycol (PEG-400) as the surfactant was added. A little aqueous solution of NaOH was dropped slowly into the solution. The nanofluid becomes stable with pH 10. To disperse nanoparticles in water, as well to break bulks and finally to gain a uniform nanofluid, the container was placed in an ultrasonic bath for 2 h. Then, the nanofluid copper oxide and deionized water were ready [35].

Figure 2 shows the suspension image after 7 days of preparation. It can be seen that the suspension is completely stable after 1 week. In the experiments, the tank, containing the suspension, has a stirrer that prepares continuous stirring during the process and prevents from settling the suspension.

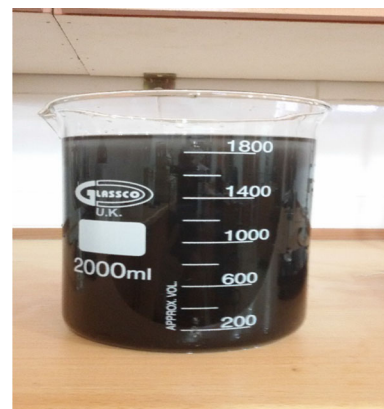


Fig. 2 Prepared CuO nanofluid solution after 7 days of preparation

Results and discussion

Synthesis of nanofluid CuO

X-ray diffraction

Figure 3 depicts the X-ray diffraction (XRD) array of CuO sample calcined at 600 °C. All of the summits in Fig. 2 are attributed to the monoclinic CuO crystallites. The average size of the calcined CuO nanoparticles was estimated by Debye–Scherrer relation [36] as below

$$D = \frac{k\lambda}{\beta \cos \theta} \quad (9)$$

that estimated to be 73 nm. The preferred peaks were observed at $2\theta = 35.6^\circ$ on page (002) and $2\theta = 38.8^\circ$ on page (111), which shows the monoclinic structure of the sample (JCPDS 80-1268).

Morphology of synthesized nanostructures

Nanostructure morphology of copper oxide was carried out using scanning electron microscopy (SEM). This technique provides locality, structure, and combination of nanoparticles by tracking a sample of the nanoparticles with an electron beam. Furthermore, SEM can recognize and analyze the fracture surface and provide information about the microstructure and surface pollution checks. As well, it is a powerful tool for studying the shape and monotony suspension. So, SEM illustration analysis gives a clear understanding of nanoparticles [37]. Figure 4 displays SEM imagery of the copper oxide nanoparticles, according to which the average size of nanoparticles was about 53 nm.

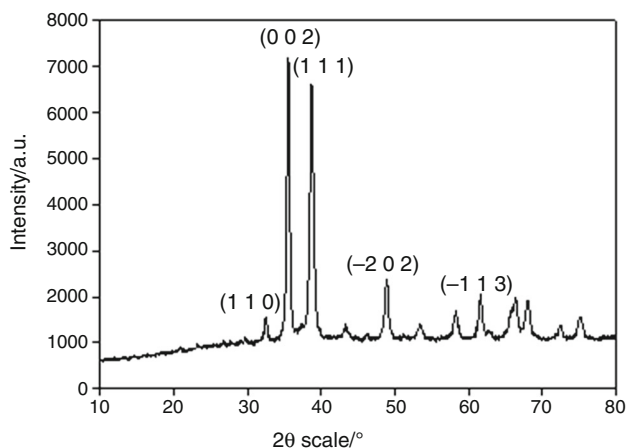


Fig. 3 X-ray diffraction pattern of CuO nanoparticles at 600 °C

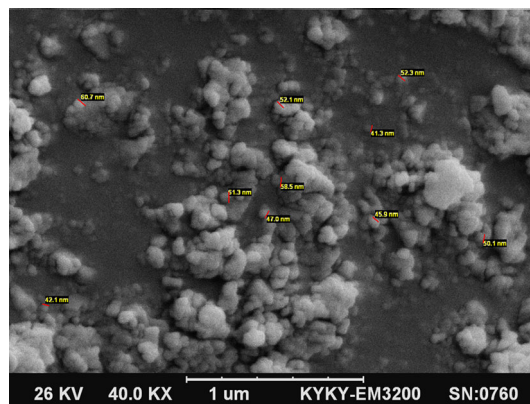


Fig. 4 SEM image of copper oxide nanoparticles

Absorption spectra of copper oxide nanoparticles

The absorption spectra of CuO nanoparticles are shown in the following forms. Absorption spectrum analysis was performed using a UV–visible. The scrolling speed was set at 20 nm min^{-1} based on the observations and results, the absorption spectrum was set at the wavelength range of 190–900 nm, and the x -axis of the absorption curve was assigned to energy. In Fig. 5, which is related to the absorption spectra of CuO nanoparticles, the absorption edge was observed at 1.4 eV and 6 eV. The band gap of the material in the bulk phase was nearly 1.4 eV in that the main absorption at 885 nm is proportional to the edges. If the absorption spectrum of this material could be measured with a UV–visible instrument at 1000 nm, the main absorption edge at 1.4 eV energy that corresponds to the band gap of this compound would be readily visible. Absorption edge (Fig. 4) has an arrow at 6 eV energy which can be attributed to one of the internal transitions.

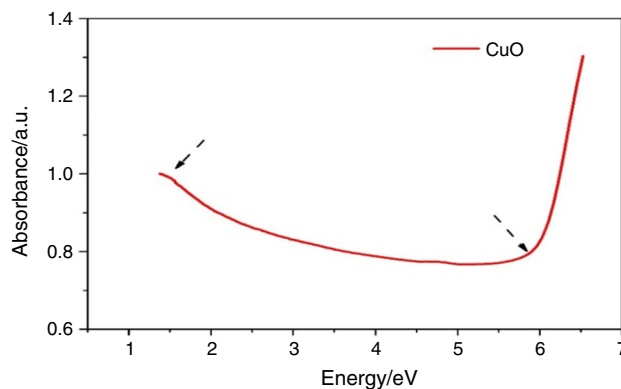


Fig. 5 Absorption spectrum of copper oxide nanoparticles

FTIR spectrum of copper oxide nanostructures

The functional groups were identified by infrared spectroscopy. Infrared spectra are vibrational–rotational spectra. Infrared spectroscopy provides more information than is usually available to the whole electronics. The presence or absence of the main absorption bands helps to detect the presence of functional groups. Figure 6 shows infrared spectroscopy of copper oxide nanoparticles. According to this figure, there are five peaks. There is a peak at 3419 cm^{-1} wave number linked on the O–H stretching of a hydroxyl group in the structure of copper oxide nanoparticles. There is a peak at 1612 cm^{-1} wave number linked on the O–H bending of a hydroxyl group in the structure of copper oxide nanoparticle. There is another peak at 1376 cm^{-1} wave number linked on the C–O asymmetric in the structure of copper oxide nanoparticle. The last peak is at 1115 cm^{-1} wave number linked on the C–O symmetric in the structure of copper oxide nanoparticle and finally, the peak in the wave number 533 cm^{-1} is related to the Cu–O bond. In addition, a peak in the wave number of 956 cm^{-1} in infrared spectroscopy is related to PEG. In infrared spectroscopy, copper oxide nanoparticles coated with polyethylene glycol are deleted, and this implies that PEG well covers the surface of the nanoparticles [38].

Application of nanofluids in the HPSC

Effect of flow rate and working fluid

Deionized water was tested in the solar collectors with the flow rates of 5, 8, 11, and 14 L min^{-1} . Also, copper oxide/deionized water nanofluid with the volume fractions of 0.008 and 0.017 was synthesized and tested with flow rates of 5, 8, 11, and 14 L min^{-1} in the HPSC. The results are

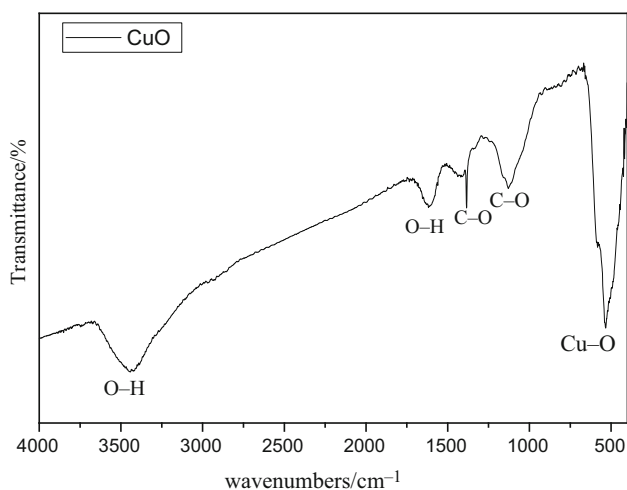


Fig. 6 FTIR spectrum of copper oxide nanoparticles

shown in Tables 2 and 3. Also, Table 4 presents the average efficiency improvement when copper oxide/deionized water nanofluid was used in the HPSC. The results showed that the efficiency is the minimum at the 5 L min^{-1} flow rate and increases from 53 to 60% as deionized water flow rate is increased to 14 L min^{-1} . Also, it was found that the maximum, average, and average increase in the collector efficiency were related to copper oxide/deionized water nanofluid with 0.017% volume fraction at 14 L min^{-1} flow rate in which they were 88.6%, 70%, and 83%, respectively. This means that the increase in nanofluid flow rate results in higher collector efficiency because of the effect of Brownian motion and increasing the collisions among particles that lead to absorb and store more heat in the nanofluid, and consequently, the collector efficiency is increased [39]. The addition of nanoparticles improved the absorption of solar radiation as compared to that of base fluid [40].

Figure 7a displays efficiency versus time graph of copper oxide/deionized water nanofluid with the flow rates of 5 and 11 L min^{-1} . According to the graph, when the nanofluid flow rate is changed from 5 to 11 L min^{-1} , the collector efficiency is increased. Figure 7b shows the efficiency versus time graph of copper oxide/deionized water nanofluid with 8 and 14 L min^{-1} flow rates. As it can be observed, when the nanofluid flow rate is increased from 8 to 14 L min^{-1} , the collector efficiency is increased. Generally, the collector efficiency is improved by increasing the flow rate of the working fluid (pure water or nanofluid). This is related to the fact that although the fluid temperature increases to a greater extent at lower flow rates than at higher flow rates due to the longer residence of the fluid in the collector, it entails more convection and radiation thermal losses [41]. Also, as Eq (1) shows, the product of the flow rate multiplied by temperature rise is so that with the increase in flow rate, more energy is absorbed and hence the efficiency is enhanced [29]. It can be concluded that the thermal performance with copper oxide/deionized water nanofluid is more than those with deionized water for all flow rates and it can be said that the collector efficiency is changed with the time and solar radiation. Improving the effective thermal conductivity (Eq. 3) is an important factor for increasing the heat transfer of conventional fluids. Since the thermal conductivity of the nanofluid is higher than of based fluids [42], when the nanofluids are used the thermal performance of solar systems is increased. Also, the absorption of the nanofluid in HPSC decreases the thermal resistance in the interface of the fluids and absorber, which reduces the temperature difference between absorber and working fluid causing an improvement in the performance. In other words, the higher thermal conductivity of a nanofluid is the

Table 2 Maximum efficiency of the use of copper oxide/deionized water nanofluids with different flow rates and the volume fractions in the HPSC

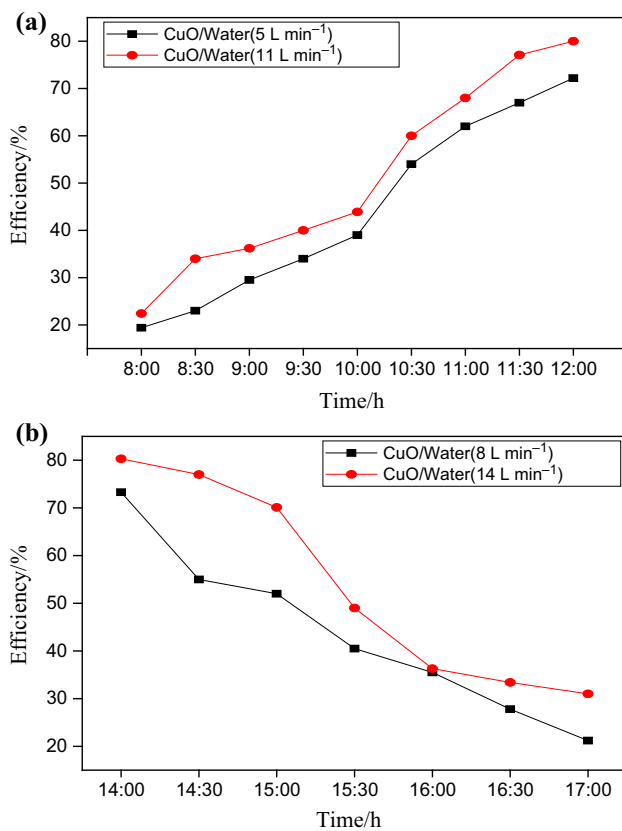
Flow rate/L/min	Deionized water	Volume fraction of 0.008%	Volume fraction of 0.017%
5	53%	72%	76%
8	54%	73%	78%
11	57%	77%	86%
14	60%	80%	88.6%

Table 3 Average efficiency of the use of copper oxide/deionized water nanofluids with different flow rates and the volume fractions in the HPSC

Flow rate/L/min	Deionized water	Volume fraction of 0.008%	Volume fraction of 0.017%
5	28%	44%	47%
8	33%	46%	50%
11	36.6%	48%	57%
14	38%	50%	70%

Table 4 Average increase the efficiency of the use of copper oxide/deionized water nanofluids with different flow rates and the volume fractions in the HPSC

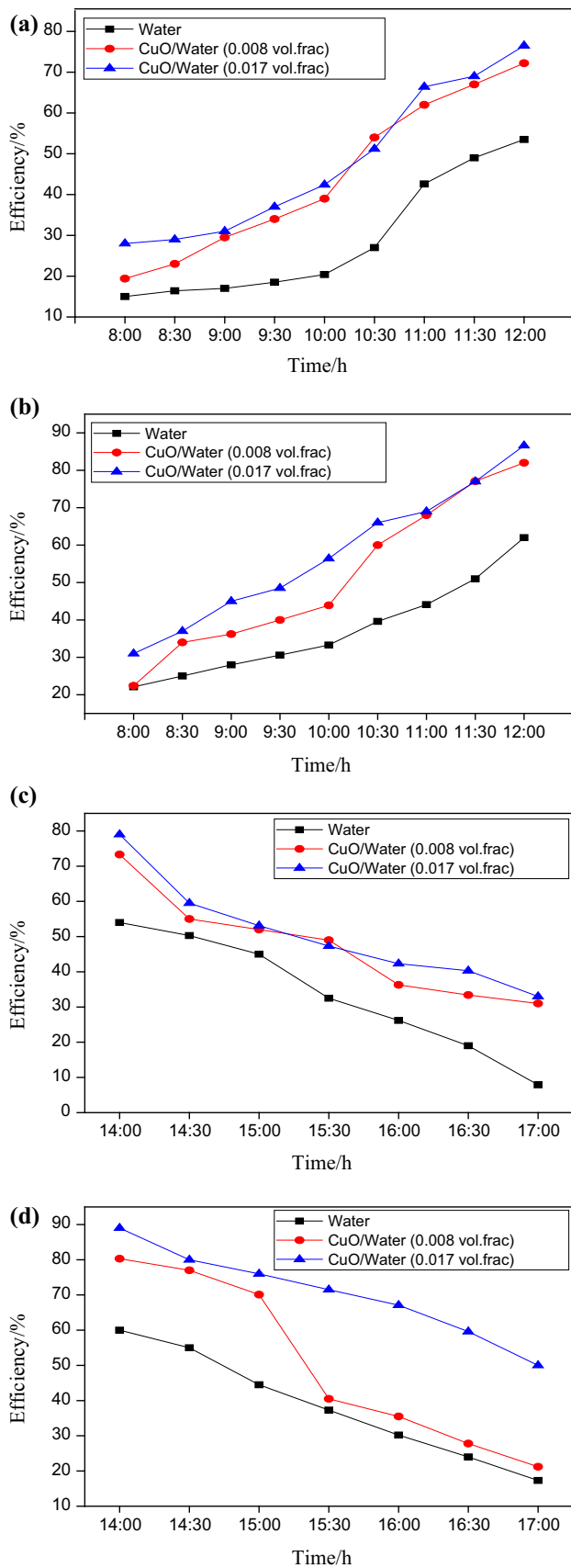
Flow rate/L/min	Volume fraction of 0.008%	Volume fraction of 0.017%
5	56%	73%
8	62%	76%
11	65%	79%
14	69%	83%

**Fig. 7** Efficiency versus time graph of copper oxide/deionized water nanofluid with flow rates: **a** 5 and 11 L min⁻¹; **b** 8 and 14 L min⁻¹

main factor for increasing the thermal performance of the solar systems [43].

Figure 8a–d depicts efficiency versus time graph of deionized water and copper oxide/deionized water nanofluid with volume fractions of 0.008% and 0.017% and with all flow rates (5, 8, 11, and 14 L min⁻¹). It can be seen that the heat transfer efficiency of the nanofluids is improved that is mainly due to higher thermal conductivity of nanoparticles. Also, by increasing the volume fraction of nanofluid, the amount of heat absorbed and stored in the nanofluid is increased which enhances the collector efficiency. As shown in Fig. 7a–d, it can be observed that due to the fraction of the incoming radiation absorbed by the fluid depends on its coefficient of damping, at a certain flow rate, by increasing the volume fraction of nanofluid, energy absorption and efficiency are increased. According to the graph, using of copper oxide/deionized water nanofluid increases the efficiency of HPSC, and the collector efficiency is increased by increasing the nanofluid volume fraction. When the volume fraction of the nanoparticle is very high, all the incoming solar radiation is absorbed through a thin surface layer where the thermal energy can easily release to the surrounding environment [39].

Eventually, it is concluded that the use of the pure water as the working fluid has lower performance, while using nanofluid with a mass fraction of 0.017% leads to the highest performance



◀Fig. 8 Efficiency versus time graph of deionized water and copper oxide/deionized water nanofluid with volume fractions of 0.008% and 0.017% and with flow rates: a 5 L min⁻¹; b 11 L min⁻¹; c 8 L min⁻¹; d 14 L min⁻¹

Analysis of uncertainty

Calculation of the experimental uncertainty is necessary for the evaluation of the assurance in the results and accomplishes a valid test. In this research, the accuracy of SMA solar meter, rotameter, and thermocouples are ± 2%, ± 0.1 L min⁻¹ and ± 0.2 °C, respectively. Moreover, the flow rate measured by using a stopwatch with ± 0.01 s accuracy and by using a graduated glass bottle of tolerance ± 1 cm³. The mean value of the two thermocouples was calculated as the experimental data. The uncertainties of the measurements, containing all the sources of errors, are listed in Table 5. The equation for uncertainty analysis is given in the following form by assuming negligible errors in density, specific heat capacity, and surface area of collector [44]

$$U_{n_{exp}} = \eta_{exp} \times \sqrt{\left(\frac{U_{\dot{m}}}{\dot{m}}\right)^2 + \left(\frac{U_G}{G}\right)^2 + \left(\frac{U_{T_o}}{T_o}\right)^2 + \left(\frac{U_{T_i}}{T_i}\right)^2}; \tag{10}$$

Therefore, the evaluations of the model showed that the maximum uncertainty in this research in obtaining the efficiency of the HPSC was about 3.2%.

The impact of environmental factors on solar collector efficiency

An external factor that affects the efficiency of the HPSC is the ambient temperature of the collector. Despite appropriate insulators, there will be a heat loss from the collector to the ambient air. Figure 9 shows the efficiency curve of $T_i - T_a / G$ where T_i is the nanofluid inlet temperature, T_a is ambient temperature of the collector, and G is the solar radiation. In this graph, the slope presents the obtained energy from the collector, which is called the utilization of energy parameter. According to this figure, the intersection of the trend with the vertical axis shows the maximum

Table 5 Uncertainty of the variables

Parameter	Uncertainty/%
inlet temperature	± 1.5
outlet temperature	± 1.5
volume flow rater	± 1.5
Solar radiation	± 2%

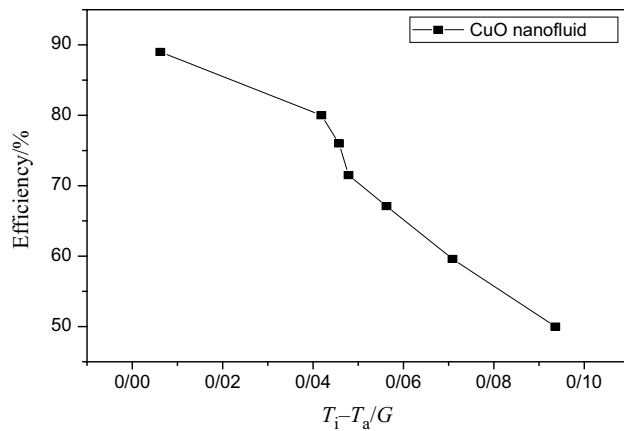


Fig. 9 Efficiency curve in terms of $T_i - T_a / G$ for **a** copper oxide/deionized water nanofluid, **b** aluminum oxide/deionized water nanofluid, **c** magnesium oxide/deionized water nanofluid

collector efficiency [44]. Therefore, if the temperature difference between the surrounding environment of the collector and inlet nanofluid is low, the collector efficiency will be high that is mainly due to dependence of collector efficiency on the $T_i - T_a / G$. Therefore, decrease in the temperature difference between the environment and inlet nanofluid collector lead to increasing the collector efficiency.

Pumping power

The effect of nanofluid on the pumping power, pressure drop, density, and viscosity for various nanoparticle volume fractions are shown in Table 6. According to Table 6, the relative pumping power, pressure drop, density, and viscosity required for the CuO nanofluid is higher than pure water, and they are enhanced by adding nanoparticles. Also, the pumping power is related to the mass flow rates, the density and the pressure drop of the working fluids. Figure 10 shows the effect of volume flow rate of working fluid and volume fraction of nanofluid CuO on the pressure drop. By increasing the volume flow rate and volume fraction of nanomaterials, the pressure drop was increased. According to Fig. 10, in the low flow rate, the pressure drop of the nanofluid is approximately equal with the base fluid. But by increasing the flow rate, the amount of

Table 6 Effect of volume fraction of copper oxide/deionized water on the density, viscosity, pressure drop, and pumping power

ϕ	$\frac{\rho_{nf}}{\rho_{bf}}$	$\frac{\mu_{nf}}{\mu_{bf}}$	$\frac{\Delta P_{nf}}{\Delta P_{bf}}$	$\frac{\dot{W}_{nf}}{\dot{W}_{bf}}$ [31]	$\frac{\dot{W}_{nf}}{\dot{W}_{bf}}$ [32]
0.008	1.04	1.02	1.03	1.03	1.03
0.017	1.09	1.04	1.07	1.07	1.05

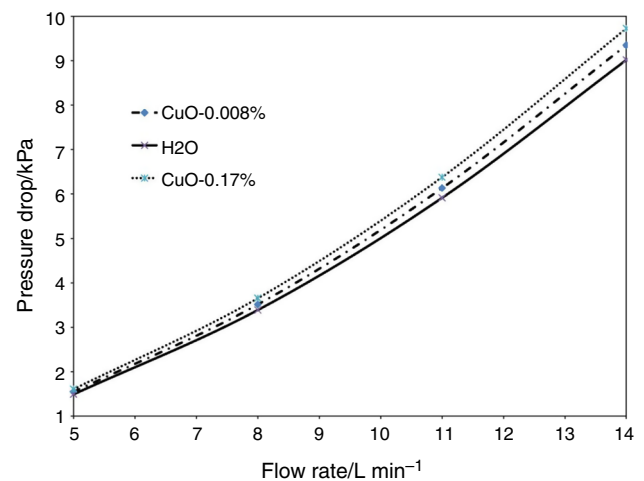


Fig. 10 Pressure drop versus volume flow rate of deionized water and copper oxide/deionized water nanofluid with volume fractions of 0.008% and 0.017%

pressure drop in the nanofluids is higher than the base fluid. However, the penalty in pressure drop and pumping power using nanofluid is so small in which it does not give any important effect on the effective performance of the solar system [45].

Conclusions

In this study, copper oxide nanoparticles were prepared by using the co-precipitation method. XRD analysis showed that the average size of CuO nanoparticles was 73 nm, and the copper oxide structure was monoclinic. Then, by using the two-step method, copper oxide/deionized water nanofluids were prepared with different volume fractions and nanofluids were used in the HPSC with different high flow rates. The performance of nanofluids in HPSC was investigated and the results showed at all flow rates, the efficiency of the HPSC with CuO nanofluid was higher than the pure water. It was also found that the nanofluid with a volume fraction of 0.017% and a flow rate of 14 L min^{-1} (0.00023 kg/s) resulted in the greatest increase in HPSC efficiency. By increasing the flow rate and volume fraction of nanofluid, the efficiency of HPSC was increased. Moreover, it was concluded that when the temperature difference between the environment and input nanofluid collector was low, the efficiency of the collector was improved.

References

1. Azad E. Assessment of three types of heat pipe solar collectors. *Renew Sustain Energy Rev.* 2012;16:2833–8.

2. Sharshir SW, Peng G, Yang N, El-Samadony MOA, Kabeel AE. A continuous desalination system using humidification–dehumidification and a solar still with an evacuated solar water heater. *Appl Therm Eng.* 2016;104:734–42.
3. Ong KS, Naghavi MS, Lim C. Thermal and electrical performance of a hybrid design of a solar-thermoelectric system. *Energy Convers Manag.* 2017;133:31–40.
4. Nkwetta DN, Smyth M, Zacharopoulos A, Hyde T. Experimental field evaluation of novel concentrator augmented solar collectors for medium temperature applications. *Appl Therm Eng.* 2013;51(1–2):1282–9.
5. Zambolin E, Del Col D. Experimental analysis of thermal performance of flat plate and evacuated tube solar collectors in stationary standard and daily conditions. *Sol Energy.* 2010;84(8):1382–96.
6. Milani D, Abbas A. Multiscale modeling and performance analysis of evacuated tube collectors for solar water heaters using diffuse flat reflector. *Renew Energy.* 2016;86:360–74.
7. He Q, Zeng Sh, Wang Sh. Experimental investigation on the efficiency of flat-plate solar collectors with nanofluids. *Appl Therm Eng.* 2015;88:165–71.
8. Leong KY, Ong HCh, Amer NH, Norazrina MJ, Risby MS. An overview on current application of nanofluids in solar thermal collector and its challenges. *Renew Sustain Energy Rev.* 2016;53:1092–105.
9. Javadi FS, Saidur R, Kamali Sarvestani M. Investigating performance improvement of solar collectors by using nanofluids. *Renew Sustain Energy Rev.* 2013;28:232–45.
10. Fuskele V, Sarviya RM. Recent developments in nanoparticles synthesis, preparation and stability of nanofluids. *Mater Today Proc.* 2017;4(2):4049–60.
11. Kakaç S, Pramuanjaroenkij A. Single-phase and two-phase treatments of convective heat transfer enhancement with nanofluids—a state-of-the-art review. *Int J Therm Sci.* 2016;100:75–97.
12. Sundar LS, Singh MK. Convective heat transfer and friction factor correlations of nanofluid in a tube and with inserts: a review. *Renew Sustain Energy Rev.* 2013;20:23–35.
13. Kumar Devendiran D, Arasu Amirtham V. A review on preparation, characterization, properties and applications of nanofluids. *Renew Sustain Energy Rev.* 2016;60:21–40.
14. Nagarajan PK, Subramani J, Suyambazhahan S, Sathyamurthy R. Nanofluids for solar collector applications: a review. *Energy Proc.* 2014;61:2416–34.
15. KadhimHussein Ahmed. Applications of nanotechnology to improve the performance of solar collectors—recent advances and overview. *Renew Sustain Energy Rev Vol.* 2016;62:767–92.
16. Muhammad MJ, Muhammad IA, Sidik NAC, Yazid MNAWM, Mamat R, Najafi G. The use of nanofluids for enhancing the thermal performance of stationary solar collectors: a review. *Renew Sustain Energy Rev.* 2016;63:226–36.
17. Daghigh R, Shafieian A. Theoretical and experimental analysis of thermal performance of a solar water heating system with evacuated tube heat pipe collector. *Appl Therm Eng.* 2016;103:1219–27.
18. Milanese M, Colangelo G, Creti A, Lomascolo M, Iacobazzi F, De Risi A. Optical absorption measurements of oxide nanoparticles for application as nanofluid in direct absorption solar power systems—part I: water-based nanofluids behavior. *Sol Energy Mater Sol Cells.* 2016;147:315–20.
19. Milanese M, Colangelo G, Creti A, Lomascolo M, Iacobazzi F, De Risi A. Optical absorption measurements of oxide nanoparticles for application as nanofluid in direct absorption solar power systems—part II: ZnO, CeO₂, Fe₂O₃ nanoparticles behavior. *Sol Energy Mater Sol Cells.* 2016;147:321–6.
20. Milanese M, Iacobazzi F, Colangelo G, de Risi A. An investigation of layering phenomenon at the liquid–solid interface in Cu and CuO based nanofluids. *Int J Heat Mass Transf.* 2016;103:564–71.
21. Colangelo G, Favale E, Milanese M, Starace G, De Risi A. Experimental measurements of Al₂O₃ and CuO nanofluids interaction with microwaves. *J Energy Eng.* 2016;143(2):04016045.
22. Mirzaei M. Experimental investigation of the assessment of Al₂O₃–H₂O and CuO–H₂O nanofluids in a solar water heating system. *J Energy Storage.* 2017;14:71–81.
23. Mahian O, Kianifar A, Kalogirou SA, Pop I, Wongwises S. A review of the applications of nanofluids in solar energy. *Int J Heat Mass Transf.* 2013;57(2):582–94.
24. Verma SK, Tiwari AK. Progress of nanofluid application in solar collectors: a review. *Energy Convers Manag.* 2015;100:324–46.
25. Moghadam AJ, Farzane-Gord M, Sajadi M, Hoseyn-Zadeh M. Effects of CuO/water nanofluid on the efficiency of a flat-plate solar collector. *Exp Thermal Fluid Sci.* 2014;58:9–14.
26. Sadri R, Hosseini M, Kazi SN, Bagheri S, Zubir N, Solangi KH, Zaharinie T, Badarudin A. A bio-based, facile approach for the preparation of covalently functionalized carbon nanotubes aqueous suspensions and their potential as heat transfer fluids. *J Colloid Interface Sci.* 2017;504:115–23.
27. Sadri R, Hosseini M, Kazi SN, Bagheri S, Abdelrazek AH, Ahmadi G, Zubir N, Ahmad R, Abidin NIZ. A facile, bio-based, novel approach for synthesis of covalently functionalized graphene nanoplatelet nano-coolants toward improved thermophysical and heat transfer properties. *J Colloid Interface Sci.* 2018;509:140–52.
28. Hosseini M, Abdelrazek AH, Sadri R, Mallah AR, Kazi SN, Chew BT, Rozali S, Yusoff N. Numerical study of turbulent heat transfer of nanofluids containing eco-friendly treated carbon nanotubes through a concentric annular heat exchanger. *Int J Heat Mass Transf.* 2018;127:403–12.
29. Gupta HK, Agrawal GD, Mathur J. Experimental study of water-based Al₂O₃ nanofluid flow in direct absorption solar collector. *Macromol Symp.* 2015;357(1):30–7.
30. Chamsa-ard W, Brundavanam S, Fung CC, Fawcett D, Poinern G. Nanofluid types, their synthesis, properties and incorporation in direct solar thermal collectors: a review. *Nanomaterials.* 2017;7(6):131.
31. Said Z, Sajid MH, Alim MA, Saidur R, Rahim NA. Experimental investigation of the thermophysical properties of Al₂O₃-nanofluid and its effect on a flat plate solar collector. *Int Commun Heat Mass Transf.* 2013;48:99–107.
32. Sadri R, Hosseini M, Kazi SN, Bagheri S, Ahmed SM, Ahmadi G, Zubir N, Sayuti M, Dahari M. Study of environmentally friendly and facile functionalization of graphene nanoplatelet and its application in convective heat transfer. *Energy Convers Manag.* 2017;150:26–36.
33. Yu W, Xie H. A review on nanofluids: preparation, stability mechanisms, and applications. *J Nanomater.* 2012;2012:1.
34. Phiw dang K, Suphan Kij S, Mekpra Sart W, Pecharapa W. Synthesis of CuO nanoparticles by precipitation method using different precursors. *Energy Proc.* 2013;34:740–5.
35. Karami M, Akhavan-Bahabadi MA, Delfani S, Raisee M. Experimental investigation of CuO nanofluid-based direct absorption solar collector for residential applications. *Renew Sustain Energy Rev.* 2015;52:793–801.
36. Siddiqui H, Qureshi MS, Haque FZ. Surfactant assisted wet chemical synthesis of copper oxide (CuO) nanostructures and their spectroscopic analysis. *Optik.* 2016;127:2740–7.
37. Sabiha MA, Saidur R, Hassani S, Said Z, Mekhilef S. Energy performance of an evacuated tube solar collector using single

- walled carbon nanotubes nanofluids. *Energy Convers Manag.* 2015;105:1377–88.
38. Sharafi A, Seyedsadjadi M. Surface-modified superparamagnetic nanoparticles Fe_3O_4 @PEG for drug delivery. *Int J Bioinorg Hybrid Nanomater.* 2013;2:437–41.
39. Saini DK, Agarwal GD. Thermo-physical properties of nanofluids—a review. *Int J Adv Eng Sci Technol.* 2019;5(1):39–45.
40. Tyagi H, Phelan P, Prasher R. Predicted efficiency of a low-temperature Nanofluid-based direct absorption solar collector. *J Sol Energy Eng.* 2009;131(4):0410041–7.
41. Bozorgi M, Karami M, Delfani S. Energy and exergy analysis of direct absorption solar collector by using silver nanofluid. *Modares Mech Eng.* 2018;18(4):814–22 (**in Persian**).
42. Gupta M, Singh V, Kumar R, Said Z. A review on thermo-physical properties of nanofluids and heat transfer applications. *Renew Sustain Energy Rev.* 2017;74:638–70.
43. Kasaeian A, Eshghi AT, Sameti M. A review on the applications of nanofluids in solar energy systems. *Renew Sustain Energy Rev.* 2015;43:584–98.
44. Mirzaei M, Hosseini SMS, Kashkooli AMM. Assessment of Al_2O_3 nanoparticles for the optimal operation of the flat plate solar collector. *Appl Therm Eng.* 2018;134:68–77.
45. Faizal M, Saidur R, Mekhilef S, Hepbasli A, Mahbubul IM. Energy, economic, and environmental analysis of a flat-plate solar collector operated with SiO_2 nanofluid. *Clean Technol Environ Policy.* 2015;17(6):1457–73.

Publisher's Note Springer Nature remains neutral with regard to jurisdictional claims in published maps and institutional affiliations.